Nanoscale avalanche photodiodes for highly sensitive and spatially resolved photon detection

OLIVER HAYDEN[1]*†, RITESH AGARWAL[1]†‡ AND CHARLES M. LIEBER[1,2]§

[1]Department of Chemistry and Chemical Biology, Harvard University, Cambridge, Massachusetts 02138, USA
[2]Department of Engineering and Applied Sciences, Harvard University, Cambridge, Massachusetts 02138, USA
*Current address: IBM Research GmbH, Zürich Research Laboratory, 8803 Rüschlikon, Switzerland
†These authors contributed equally to the work
‡Current address: Department of Materials Science and Engineering, University of Pennsylvania, Philadelphia, Pennsylvania 19104-6272, USA
§e-mail: cml@cmliris.harvard.edu

Published online: 16 April 2006; doi:10.1038/nmat1635

Integrating nanophotonics with electronics could enhance and/or enable opportunities in areas ranging from communications and computing to novel diagnostics[1,2]. Light sources and detectors are important elements for integration[1], and key progress has been made using semiconducting nanowires[3–5] and carbon nanotubes to yield electrically driven sources[6–12] and photoconductor detectors[13–17]. Detection with photoconductors has relatively poor sensitivity at the nanometre scale, and thus large amplification is required to detect low light levels and ultimately single photons with reasonable response time. Here, we report avalanche multiplication of the photocurrent in nanoscale p–n diodes consisting of crossed silicon–cadmium sulphide nanowires. Electrical transport and optical measurements demonstrate that the nanowire avalanche photodiodes (nanoAPDs) have ultrahigh sensitivity with detection limits of less than 100 photons, and subwavelength spatial resolution of at least 250 nm. Crossed nanowire arrays also show that nanoAPDs are reproducible and can be addressed independently without cross-talk. NanoAPDs and arrays could open new opportunities for ultradense integrated systems, sensing and imaging applications.

The nanoAPDs were assembled by sequential fluid-directed assembly[18] of solutions of n-CdS and p-Si nanowires[8,9], and independent electrical contacts were defined by lithography and metal deposition (see the Methods section) as described previously[9]. We have focused our efforts on crossed-nanowire p–n structures for several reasons, including the ability to (1) independently tune dopant concentration in the p-silicon nanowires[10,11] while maintaining a high absorption coefficient with the n-CdS nanowires, and (2) define abrupt, nanoscale junctions that are ideal for high spatial resolution. The dark current (I_{dark}) as a function of bias voltage recorded from a representative device shown in Fig. 1a shows a sharp increase in $|I_{dark}|$ at approximately -9 V. Illumination of the same device shows a voltage-dependent photocurrent (I_{ph}) that increases with increasing negative reverse bias until $I_{ph} \approx I_{dark}$ at -10 V, which is suggestive of an avalanche breakdown process[19]. More detailed measurements shown in Fig. 1b demonstrate that I_{dark} remains constant at $\sim$100 pA until breakdown occurs at -9 V.

We have used these data to calculate the multiplication factor, M, for the nanoAPD using McIntyre's formula[20]: $M = (I_{ph} - I_{dark})/I_{ug}$, where I_{ug} is the unity gain ($M = 1$) of the photocurrent. The plot of M versus bias voltage in Fig. 1b shows that this device exhibits a multiplication factor of about 5×10^4 for sub-breakdown biases. Studies of a number of similar n-CdS/p-Si crossed nanowire devices demonstrate that this high multiplication is reproducible, with values of M as large as 7×10^4 observed. In contrast, single n-CdS or p-Si nanowire devices exhibit maximum photoconductive gain (I_{ph}/I_{dark}) of only 3–5 (see the Supplementary Information) or approximately 10,000 times lower than our nanoAPDs. Hence, the high gain observed cannot be the result of photoconductivity in the individual nanowires, but must result from an amplification process associated with the p–n diode formed at the crossed-nanowire junction.

To further characterize the nature of amplification in crossed-nanowire structures, we have made spatially resolved photocurrent measurements. As shown in Fig. 1c, a highly localized photocurrent peak is observed in scanning photocurrent measurements, where the I_{ph} peak is located at the position of the reverse-biased p–n crossed-nanowire junction. No gain is observed at the nanowire electrode contacts, which is distinct from previous studies[16] where contact barriers have dominated the response. These results clearly demonstrate that amplification is associated with the nanoscale p–n junction. In addition, measurements of the spectral response show that the CdS nanowire is the predominant absorbing medium

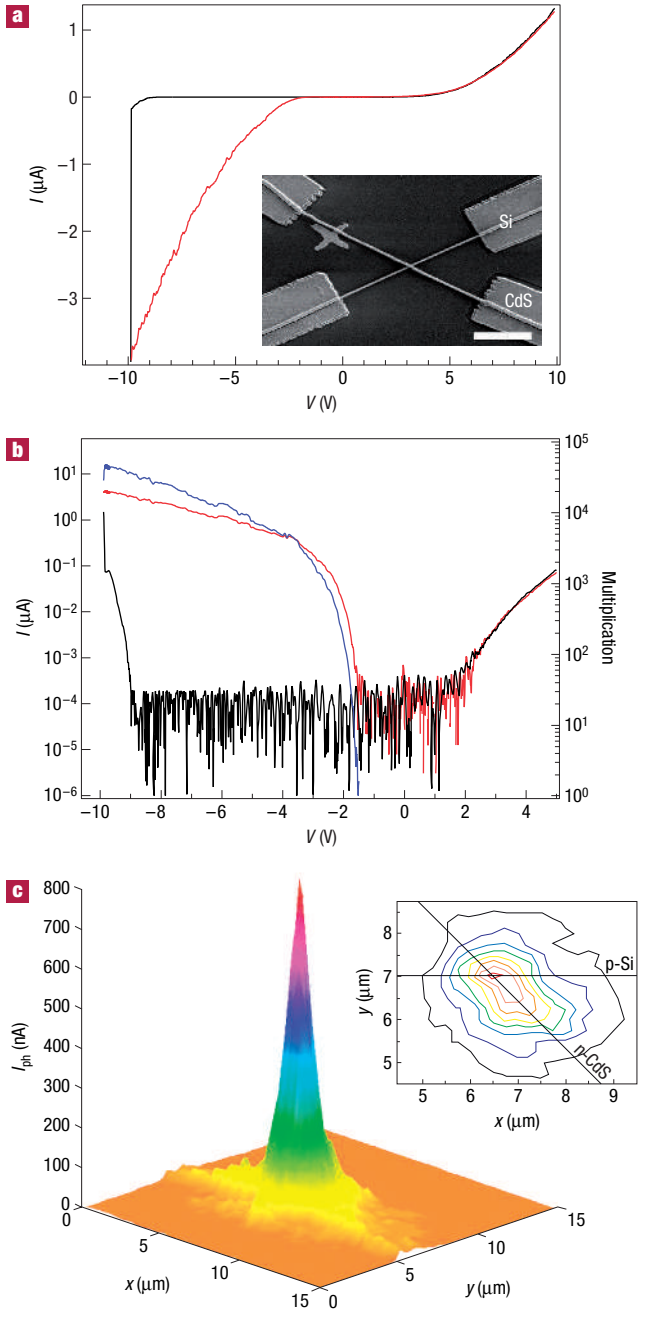

Figure 1 Characterization of nanowire APDs. a, *I–V* characteristic of the APD in dark (black line) and illuminated (red line) conditions; the device was illuminated with 500 nW of 488-nm light (red line). The inset shows a scanning electron micrograph of the n-CdS/p-Si device; the scale bar is 4 μm. **b**, Logarithmic scale APD *I–V* characteristics (black line: dark; red line: illuminated) and corresponding multiplication factor (blue line). **c**, Plot of the spatially resolved photocurrent from the nanoAPD measured in the proportional mode using a diffraction-limited laser; the bias voltage, laser power and scanning step size were −7 V, 200 nW and 250 nm (in *x* and *y*), respectively. The inset shows a contour plot with slices taken every 100 nA. The nanowire positions are indicated on the plot by solid lines.

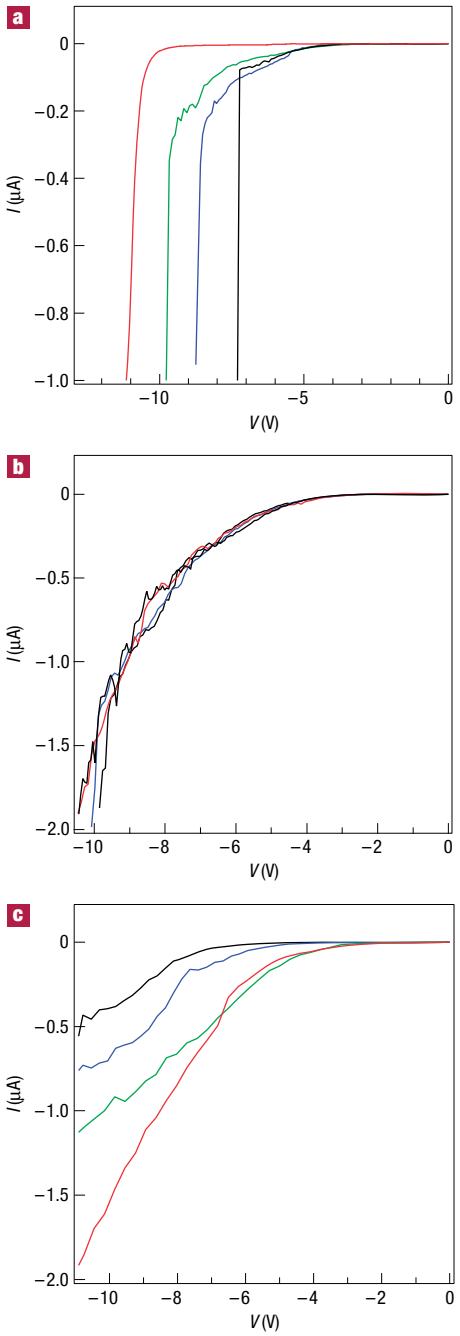

Figure 2 Temperature-dependent *I–V* for n-CdS/p-Si crossed-nanowire APDs as a function of p-Si dopant level. The *I–V* data were recorded at 75 (black lines), 150 (blue lines), 225 (green lines) and 300 K (red lines) for devices in which B_2H_6:SiH_4 gas ratios during synthesis were **a**, 1:6,000, **b**, 1:4,000 and **c**, 1:250, where B_2H_6 is the p-type dopant; the CdS nanowires had the same intrinsic doping level in all three devices.

with a maximum photocurrent for wavelengths at the CdS bandgap (see the Supplementary Information); the spectral response is consistent with photocurrent studies made on single-crystal CdS[21].

Analysis of the I_{ph} position data further shows that the spatial resolution of the device is at least 250 nm, the step size used in the scanning experiment. Significantly, these results demonstrate that the detector has subwavelength resolution in addition to very high gain.

To determine the photodiode breakdown mechanism, temperature-dependent transport studies of crossed n-CdS/p-Si

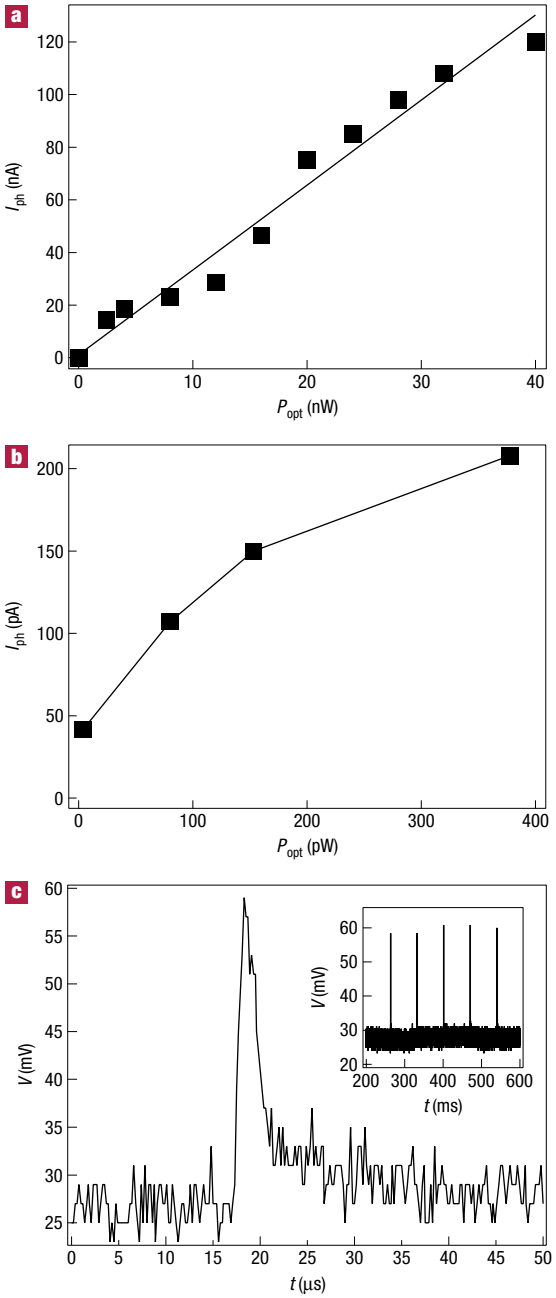

Figure 3 Crossed-nanowire APD responsivity. a,**b**, Detection sensitivity measured at room temperature using a calibrated photon source. The device was biased at −8 V, and the calibrated output from a frequency doubled Ti:sapphire laser at 400 nm (250-fs pulses; 76-MHz repetition rate) was used as a source. **c**, Temporal response of the crossed nanowire APD recorded using a frequency tripled Nd:YAG laser (355 nm; 10-ns pulse width; 16 Hz). The inset shows a train of photocurrent peaks concurrent with the laser pulses.

nanowire devices were carried out. Figure 2a shows that the pronounced breakdown shifts to higher absolute voltages as temperature increases. This positive temperature coefficient of about +15 mV K^{-1} and the 'hard-knee' breakdown is a clear signature of an avalanche breakdown mechanism[19]. For comparison, avalanche photodiodes from II–VI wide bandgap ZnSe semiconductor have a temperature dependence of about +23 mV K^{-1} (ref. 22). Further support for this interpretation was obtained through temperature-dependent transport measurements on structures assembled using p-Si nanowires with higher dopant concentrations. We varied the boron dopant concentration by growing silicon nanowires with different B_2H_6:SiH_4 ratios. Previous work[10,11] has shown that this leads to systematic changes in the effective dopant concentration from about 2×10^{18} cm^{-3} to 2 to 3×10^{19} cm^{-3}. Measurement on crossed-nanowire devices assembled using p-Si nanowire growth with the B_2H_6:SiH_4 = 1:4,000 showed a much more gradual (soft-knee) and temperature-independent breakdown mechanism in crossed-nanowire photodiodes (Fig. 2b). Notably, devices assembled using nanowires grown with a B_2H_6:SiH_4 = 1:250 yielded a soft-knee breakdown but showed a shift to lower voltages with increasing temperature at a rate of about −10 mV K^{-1} (Fig. 2c). This negative temperature dependence is characteristic of a Zener breakdown mechanism[19], and distinct from that observed in devices showing high multiplication. Taken together, these studies provide clear evidence that the high gain of the crossed-nanowire photodiodes is the result of an avalanche mechanism.

The photon-detection limits of our nanoAPDs were determined using a calibrated laser excitation source (see the Methods section). Data shown in Fig. 3a,b demonstrate a large dynamic range from pW to nW. The lowest power that was easily measured above the noise level was 4 pW, corresponding to an estimated detection limit of about 75 photons. This very high sensitivity can be attributed to the large avalanche multiplication effect, which compensates for the low photon absorption cross-section of these nanoscale photodetectors, and yields significant improvements compared with nanowire photodetectors without carrier amplification, such as photoconductors[13] and metal–semiconductor–metal detectors[16]. In addition, it should be possible to achieve higher sensitivities by, for example, using core/shell nanowire structures[12,23] to assemble p–i–n junctions for improved field strength and gain. Ultimately, single-photon detectability might be obtained using the Geiger mode of an actively or passively quenched nanoAPD[24].

We also investigated the temporal response of the nanoAPDs. For example, the inset of Fig. 3c shows a train of photocurrent pulses that are concurrent with the incident laser pulses. Analysis of a single photocurrent peak in Fig. 3c yields a 90%–10% fall time of about 3 μs. The time fluctuation between photon absorption and electrical detection is <2 μs (amplifier-limited rise time). This time constant is limited by instrument response, and does not represent the intrinsic speed of the nanoAPD. Nevertheless, this measured value is five times faster than a recently reported single nanowire photodetector[16], but considerably slower than comparatively large-area commercial Si APDs[25]. A better measure of the intrinsic nanoAPD response time could be obtained in the future by using techniques, such as photocurrent correlation measurements, that are not limited by the gain bandwidth of the electrical measurement systems. In addition, smaller electrode distances as well as the passivation of surface traps could be used to enhance the temporal response time of these devices.

One potential advantage of our crossed-nanowire devices is that the architecture can be extended to arrays with independently addressable devices. To demonstrate this concept, we investigated an array consisting of two silicon nanowires crossing a single CdS nanowire as shown in Fig. 4a. Scanning photocurrent data acquired from this array (Fig. 4b) showed two well-defined photocurrent peaks that were located at the positions of the individual nanoAPDs (Fig. 4b). The two device elements in the array exhibited spatial resolution and gain similar to the single nanoAPDs described above. Importantly, the similar sensitivity of the elements within the array and compared to single devices in Fig. 1 testify to

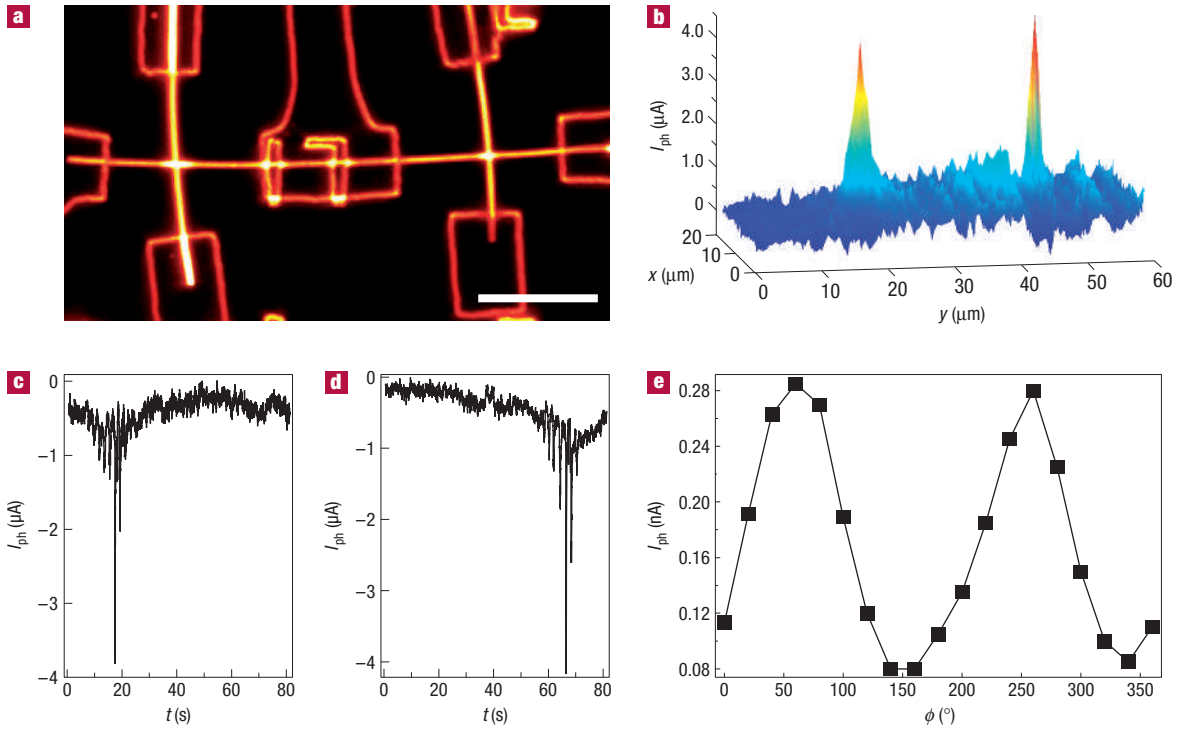

Figure 4 Nanowire APD arrays. a, Optical micrograph of an array consisting of an n-CdS nanowire (horizontal) crossing two p-Si nanowires (vertical); the larger rectangular features correspond to metal contacts (scale bar, 10 μm). **b**, Spatially resolved photocurrent measured from the array in **a**. Both devices were biased at −10 V and excited at 488 nm (200 nW, Ar^+-ion laser) with a scanning step size of 1 μm. **c**,**d**, I_{ph} versus time traces for laser scanning measurements where individual devices were turned on (biased at −10 V); the left device is on in **c** and the right device on in **d**. **e**, I_{ph} versus polarization (ϕ) for a nanowire APD (see the Methods section); the device was biased at −5 V.

the reproducibility of the nanoAPDs prepared by our relatively simple approach.

In addition, analysis of I_{ph} time traces (Fig. 4c,d), with the equal starting point and dwell time for the raster scans, demonstrate that the nanoAPD elements in the array can be independently turned on and off, and that there is no electrical cross-talk between the two devices when only one is illuminated. It is also worth considering the prospects for larger arrays, although we stress that single nanoAPDs represent a unique advance and could have important applications without the need for arrays. We have made arrays with up to three elements that show independent detection (no cross-talk) with device separations on a similar 10-μm scale as that above. It should be possible to push the separation to about the 1 μm scale without modifications of our approach by using the spatially resolved photocurrent peak (for example, Fig. 1c) as an estimate of carrier collection length. However, one may be able to improve this device separation by using axial nanowire heterostructures[3,4,10], which can effectively isolate each element while keeping the basic crossed nanowire array structure.

Lastly, the polarization-dependent I_{ph} measurements shown in Fig. 4e demonstrate that the nanoAPD response is highly sensitive to the polarization of the detected light. Quantitative analysis of the results shows that polarization ratios of the order of 56% can be obtained for our devices, and are reproducible. The polarization contrast observed is lower than that expected for a fully isolated nanowire, 75%, on the basis of the dielectric contrast between the nanowire ($\varepsilon = 7.2$) and the surrounding medium ($\varepsilon \sim 1.0$) (ref. 13). The lower polarization contrast in real devices is expected due to factors not accounted for in the simple model including, coupling to the substrate, the finite diameter of CdS nanowires, and the crossed-silicon nanowire component of the device. Nevertheless, the 56% polarization ratio represents a unique feature compared with conventional APDs that require additional optical elements to achieve polarization sensitivity.

Our studies describe the first nanoscale APDs, where the devices have been developed in a general way from crossed p-silicon and n-cadmium sulphide nanowire diodes. The nanoAPDs exhibit ultrahigh sensitivity with detection limits of less than 100 photons, subwavelength spatial resolution of at least 250 nm, excellent polarization sensitivity, and can be assembled into small arrays in which the nanoAPD elements are reproducible and can be addressed independently without cross-talk. These results represent a significant advance over existing nanoscale photodetectors[13–16], especially in terms of sensitivity and spatial resolution, and moreover, nanoAPD sensitivity (below breakdown voltage) is comparable to that reported for conventional planar APD structures[26]. Our approach is flexible and should enable nanoAPDs to be configured from distinct semiconductor nanowire materials, which could tailor sensitivity in specific spectral regions, and also to improve detection sensitivity and device stability by using core/shell nanowire structures to enhance gain. We believe that the features demonstrated for the nanoAPDs in these studies offer substantial promise in diverse areas ranging from nanopositioning, integrated photonics, and near-field detection to real-time observation of single protein dynamics with integrated nanoAPDs in microfluidics[27] and the potential for polarization-dependent single photon counting in the Geiger mode[24].

METHODS

DEVICE FABRICATION

CdS nanowires with diameters ranging from 80 to 150 nm and Si nanowires with 50-nm diameters were grown by means of a metal nanocluster catalysed growth approach described previously[8,9,27]. The effective doping level of the p-Si nanowires was varied by the ratio of B_2H_6:SiH_4 in the reactor. Crossed n-CdS and p-Si nanowire structures were prepared by microfluidic-directed assembly[18] using orthogonal sequential flows of the CdS and Si nanowires. Electron-beam lithography was used to pattern electrodes at the ends of crossed nanowire structures, and titanium contacts (100 nm) were deposited by electron-beam evaporation. All of the devices were fabricated on oxidized Si (600-nm thermal SiO_2) substrates.

SPATIALLY RESOLVED PHOTOCURRENT MEASUREMENTS

Scanning photocurrent measurements were carried out by focusing the 488-nm line of the Ar-ion laser beam with a 0.9-NA objective to a spot size of ~500 nm. The spatially resolved photocurrent was measured by raster scanning (step size of 250 nm) the sample using a Digital PI PZT flexure stage.

PHOTODIODE SENSITIVITY

The lowest average optical power for which we could measure a response above the noise level measured was 4 pW (400 nm, pulse repetition rate 76 MHz), corresponding to an average of approximately 0.1 photons per pulse. The data were collected with an instrument-resolution-limited photocurrent rise time of 10 ms, which corresponds to 760,000 laser pulses impinging on the photodetector during the 10-ms time interval. The laser was focused to a spot size of 3 μm. For the CdS nanowire of ~100-nm diameter, the calculated area fraction of the nanowire (area of the nanowire/area of the laser spot) is ~0.01, that is, 1% of the laser energy interacts with the nanowire. On the basis of the absorption coefficient of CdS at 488 nm ($\sim 10^5$) followed by calibration from the photocurrent spectrum in Fig. 3b for absorption efficiency at 400 nm, it is estimated that ~10% of the incident light will be absorbed by the 100-nm-thick CdS nanowire. Therefore, on the basis of the area fraction and absorption efficiency of CdS nanowire at 400 nm, we estimate that ~0.1% of the total number of photons impinging on the detector will be effectively absorbed. This leads to an estimation of ~76 photons absorbed by the CdS nanowire ($760{,}000 \times 0.1 \times 0.001$) to produce a measurable photocurrent response.

In addition, we have used the 1-μm full-width at half-maximum value determined from the spatially scanned photocurrent measurements as an approximation of the depletion width (×2). This will yield somewhat higher sensitivity than our conservative model above because the signal is arising from a smaller number of photons. In addition, using the effective donor concentration in the CdS nanowires of about 5×10^{17} cm^{-3} (from transport measurements), and assuming that there are approximately the same concentration of donors and acceptors, yields a consistent depletion width of around ~0.5 μm at a bias of 8 V.

Received 22 December 2005; accepted 16 March 2006; published 16 April 2006.

References

1. Saleh, B. E. A. & Teich, M. C. (eds) *Fundamentals of Photonics* (Wiley, New York, 1991).
2. Prasad, P. N. (ed.) *Elements of Nanophotonics* (Wiley, New York, 2004).
3. Lieber, C. M. Nanoscale science and technology: Building a big future from small things. *Mater. Res. Soc. Bull.* **28,** 486–491 (2003).
4. Samuelson, L. *et al.* Semiconductor nanowires for 0D and 1D physics and applications. *Physica E* **25,** 313–318 (2004).
5. Bakkers, E. P. A. M. *et al.* Epitaxial growth of InP nanowires on germanium. *Nature Mater.* **3,** 769–773 (2004).
6. Duan, X., Huang, Y., Cui, Y., Wang, J. & Lieber, C. M. Indium phosphide nanowires as building blocks for nanoscale electronic and optoelectronic devices. *Nature* **409,** 66–69 (2001).
7. Misewich, J. A. *et al.* Electrically induced optical emission from a carbon nanotube FET. *Science* **300,** 783–786 (2003).
8. Duan, X., Huang, Y., Agarwal, R. & Lieber, C. M. Single-nanowire electrically driven lasers. *Nature* **421,** 241–245 (2003).
9. Huang, Y., Duan, X. & Lieber, C. M. Nanowires for integrated multicolor nanophotonics. *Small* **1,** 142–147 (2005).
10. Wu, Y., Xiang, J., Yang, C., Lu, W. & Lieber, C. M. Single-crystal metallic nanowires and metal/semiconductor nanowire heterostructures. *Nature* **430,** 61–65 (2004).
11. Lew, K.-K. *et al.* Structural and electrical properties of trimethylboron-doped silicon nanowires. *Appl. Phys. Lett.* **85,** 3101–3103 (2004).
12. Qian, F., Gradecak, S., Li, Y., Wen, C.-Y. & Lieber, C. M. Core/multishell nanowire heterostructures as multicolor, high-efficiency light-emitting diodes. *Nano Lett.* **5,** 2287–2291 (2005).
13. Wang, J., Gudiksen, M. S., Duan, X., Cui, Y. & Lieber, C. M. Highly polarized photoluminescence and photodetection from single indium phosphide nanowires. *Science* **293,** 1455–1457 (2001).
14. Kind, H., Yan, H., Messer, B., Law, M. & Yang, P. Nanowire ultraviolet photodetectors and optical switches. *Adv. Mater.* **14,** 158–160 (2002).
15. Freitag, M., Martin, Y., Misewich, J. A., Martel, R. & Avouris, Ph. Photoconductivity of single carbon nanotubes. *Nano Lett.* **3,** 1067–1071 (2003).
16. Gu, Y. *et al.* Near-field scanning photocurrent microscopy of a nanowire photodetector. *Appl. Phys. Lett.* **87,** 043111 (2005).
17. He, J. H., Lao, C. S., Chen, L. J., Davidovic, D. & Wang, Z. L. Large-scale Ni-doped ZnO nanowire arrays and electrical and optical properties. *J. Am. Chem. Soc.* **127,** 16376–16377 (2005).
18. Huang, Y., Duan, X., Wei, Q. & Lieber, C. M. Directed assembly of one-dimensional nanostructures into functional networks. *Science* **291,** 630–633 (2001).
19. Seymour, J. (ed.) *Electronic Devices & Components* (Longman Scientific and Technical, Essex, 1988).
20. Yuan, P. *et al.* A new look at impact ionization-part II: Gain and noise in short avalanche photodiodes. *IEEE Trans. Electron Devices* **46,** 1632–1639 (1999).
21. Shin, Y. J. *et al.* Photocurrent study on the splitting of the valence band for a CdS single crystal platelet. *Phys. Rev. B* **44,** 5522–5526 (1991).
22. Abe, T. *et al.* Demonstration of blue-ultraviolet avalanche photodiodes of II-VI wide bandgap compounds grown by MBE. *J. Cryst. Growth* **214–215,** 1134–1137 (2000).
23. Lauhon, L. J., Gudiksen, M. S., Wang, D. & Lieber, C. M. Epitaxial core–shell and core–multishell nanowire heterostructures. *Nature* **420,** 57–61 (2002).
24. Brown, R. G. W., Ridley, K. D. & Rarity, J. G. Characterization of silicon avalanche photodiodes for photon correlation measurements. 1: Passive quenching. *Appl. Opt.* **25,** 4122–4126 (1986).
25. Campbell, J. C. *et al.* Recent advances in avalanche photodiodes. *IEEE J. Sel. Top. Quantum Electron.* **10,** 777–797 (2002).
26. Sun, X. & Davidson, F. M. Photon counting with silicon avalanche photodiodes. *J. Lightwave Technol.* **10,** 1023–1032 (1992).
27. Hayden, O. & Payne, C. K. Nanophotonic light sources for fluorescence spectroscopy and cellular imaging. *Angew. Chem. Int. Edn* **44,** 1395–1398 (2005).

Acknowledgements

We thank W. Riess for discussions. We gratefully acknowledge the assistance of H. Babcock and J. Xiang, and we thank X. Zhuang for the use of their optical microscope system.
Correspondence and requests for materials should be addressed to C.M.L.
Supplementary Information accompanies this paper on www.nature.com/naturematerials.

Competing financial interests

The authors declare that they have no competing financial interests.